Journal of Bacteriology

# The Peptidoglycan Sacculus of *Myxococcus xanthus* Has Unusual Structural Features and Is Degraded during Glycerol-Induced Myxospore Development

**Nhat Khai Bui, Joe Gray, Heinz Schwarz, Peter Schumann, Didier Blanot and Waldemar Vollmer**

***J. Bacteriol.*** **2009, 191(2):494. DOI: 10.1128/JB.00608-08.**
**Published Ahead of Print 7 November 2008.**

JOURNAL OF BACTERIOLOGY, Jan. 2009, p. 494–505 Vol. 191, No. 2
0021-9193/09/$08.00+0 doi:10.1128/JB.00608-08


# The Peptidoglycan Sacculus of *Myxococcus xanthus* Has Unusual Structural Features and Is Degraded during Glycerol-Induced Myxospore Development[▽]

Nhat Khai Bui,[1] Joe Gray,[2] Heinz Schwarz,[3] Peter Schumann,[4] Didier Blanot,[5] and Waldemar Vollmer[1]*

*Institute for Cell and Molecular Biosciences, Newcastle University, Framlington Place, Newcastle upon Tyne NE2 4HH, United Kingdom[1]; ICaMB Pinnacle Lab, Newcastle University, Framlington Place, Newcastle upon Tyne NE2 4HH, United Kingdom[2]; Max Planck Institute for Developmental Biology, Spemannstrasse 35, 72076 Tübingen, Germany[3]; DSMZ-Deutsche Sammlung von Mikroorganismen und Zellkulturen GmbH, Inhoffenstraße 7B, 38124 Braunschweig, Germany[4]; and Enveloppes Bactériennes et Antibiotiques, IBBMC, UMR 8619 CNRS, Université Paris-Sud, Orsay, France[5]*

Received 1 May 2008/Accepted 19 October 2008

**Upon nutrient limitation cells of the swarming soil bacterium *Myxococcus xanthus* form a multicellular fruiting body in which a fraction of the cells develop into myxospores. Spore development includes the transition from a rod-shaped vegetative cell to a spherical myxospore and so is expected to be accompanied by changes in the bacterial cell envelope. Peptidoglycan is the shape-determining structure in the cell envelope of most bacteria, including myxobacteria. We analyzed the composition of peptidoglycan isolated from *M. xanthus*. While the basic structural elements of peptidoglycan in myxobacteria were identical to those in other gram-negative bacteria, the peptidoglycan of *M. xanthus* had unique structural features. *meso*- or LL-diaminopimelic acid was present in the stem peptides, and a new modification of *N*-acetylmuramic acid was detected in a fraction of the muropeptides. Peptidoglycan formed a continuous, bag-shaped sacculus in vegetative cells. The sacculus was degraded during the transition from vegetative cells to glycerol-induced myxospores. The spherical, bag-shaped coats isolated from glycerol-induced spores contained no detectable muropeptides, but they contained small amounts of *N*-acetylmuramic acid and *meso*-diaminopimelic acid.**

*Myxococcus xanthus* is a rod-shaped, gram-negative soil bacterium with a complex life cycle and is a model for bacterial multicellular organization and differentiation (20, 37). Under nutrient-limiting conditions on solid media, *M. xanthus* vegetative cells aggregate to form fruiting bodies consisting of hundreds of thousands of cells in a highly coordinated way (23). During fruiting body formation the majority of cells (ca. 80%) lyse by programmed cell death mediated by the toxin MazF (27). About 20% of the cells develop into spherical myxospores which are better adapted to deleterious environmental conditions than vegetative cells (42, 54). Myxospore formation takes about 48 h in a fruiting body. In liquid culture addition of 0.5 M glycerol to the growth medium stimulates vegetative cells to form myxospores within a few hours (10). Glycerol-induced myxospores resemble the spores formed in fruiting bodies with respect to gross morphology and resistance properties; however, the two types of spores differ in important respects. For example, spores obtained using glycerol induction lack the major cell surface protein (protein S) present in spores that develop in fruiting bodies (18). The induction of myxospore formation in liquid culture has also permitted detection of changes in intermediary metabolism (22, 31, 32, 49), as well as variations in the synthesis of macromolecules (1, 12, 13, 19, 30, 39, 52, 55) that occur during development.

The cell shape of most bacteria is determined by the shape of the peptidoglycan (murein) sacculus, an exoskeleton surrounding the cytoplasmic membrane that is essential for osmotic stability (46, 51). The only previous study of peptidoglycan from *M. xanthus* was published about 40 years ago (52). This study showed that the amino sugar and amino acid composition of *M. xanthus* peptidoglycan is similar to the amino sugar and amino acid compositions of peptidoglycans of other gram-negative bacteria. The same study reported that, surprisingly and in contrast to peptidoglycan sacculi from other species, sacculi from *M. xanthus* disintegrated when they were incubated with trypsin or sodium dodecyl sulfate (SDS) (52). Based on these findings, it was suggested that the cell envelope of *M. xanthus* could contain patches of discontinuous peptidoglycan separated by other material rather than a continuous peptidoglycan sacculus (52). Given the essential role that peptidoglycan plays in determining cell shape, the morphological change from a rod-shaped *M. xanthus* vegetative cell to a spherical myxospore is expected to be paralleled by major changes in the shape and/or composition of the peptidoglycan sacculus. Indeed, previous work demonstrated that there was a decrease in peptide cross-linkage during glycerol-induced myxospore formation (52).

In this work we performed an analysis of the peptidoglycan sacculus of vegetative cells and glycerol-induced myxospores of *M. xanthus*. We found that vegetative cells contained peptidoglycan with unusual structural features that formed a bag-

* Corresponding author. Mailing address: Institute for Cell and Molecular Biosciences, Medical School, University of Newcastle upon Tyne, Catherine Cookson Building, Framlington Place, Newcastle upon Tyne NE2 4HH, United Kingdom. Phone: 44-(0)191-222 6295. Fax: 44-(0)191-222 7424. E-mail: W.Vollmer@ncl.ac.uk.

▽ Published ahead of print on 7 November 2008.

shaped sacculus. Furthermore, the peptidoglycan was degraded during the transition to glycerol-induced myxospores. These spores had a bag-shaped envelope, the spore coat.

## MATERIALS AND METHODS

**Strains and growth conditions.** *M. xanthus* DK1622 GJV1 (11) was grown at 30°C in CTT medium (1% Casitone [Gibco], 8 mM $MgSO_4$, 1 mM potassium phosphate, 10 mM Tris-HCl; pH 7.6) in liquid cultures in shaking flasks or on CTT-0.5% agar plates. For induction of myxospore formation 0.5 M glycerol was added to a liquid culture of vegetative cells with an optical density of 0.2 to 0.6, which was followed by continuous incubation at 30°C. Inspection of samples by light microscopy showed that more than 95% of the induced cells developed into glycerol-induced myxospores within 2.5 to 3 h.

**Isolation of peptidoglycan.** *M. xanthus* cells from a culture with an optical density of 0.4 to 0.8 which had been grown for 2.5 to 3 h in the presence or absence of 0.5 M glycerol were sedimented, resuspended in ice-cold water, and dropped into the same volume of boiling 5% SDS. Purification of peptidoglycan for high-performance liquid chromatography (HPLC) or HPLC-mass spectrometry (MS) analysis was performed as described previously for *Escherichia coli* (14, 15, 25). Some sacculus preparations were treated with 100 mM NaOH for 2 h to release alkaline-labile modifications and were then washed three times with water and resuspended in water. Sacculi were prepared for electron microscopy by using a procedure described previously by de Pedro et al. (8).

**Preparation and HPLC separation of muropeptides.** Muropeptides were released from sacculi with cellosyl, reduced by using sodium borohydride, and separated by reversed-phase HPLC as previously described (14). Some spore coats were mechanically broken with glass beads (0.17 to 0.18 mm; Sigma) in a FastPrep machine. If muropeptides were prepared for MS analysis, the digestion buffer used was 20 mM ammonium acetate (pH 4.8) and the reduction step was omitted.

**Offline electrospray MS.** Muropeptide HPLC fractions (0.5 ml) were concentrated in vacuo to 20 μl and then acidified by addition of 10% trifluoroacetic acid (2 μl). All samples were desalted using RP-$C_{18}$ StageTips (Proxeon Biosytems, Odense, Denmark) and eluted with a 60% acetonitrile-0.2% formic acid solution (10 μl). The muropeptide eluate was loaded into a medium NanoES spray capillary (Proxeon) and then analyzed by nano-electrospray MS in positive ion mode using a Finnigan LTQ-FT Fourier transform (FT) mass spectrometer (ThermoElectron, Bremen, Germany). The mass spectrometer was used to perform survey MS scans over the mass range from $m/z = 300$ to $m/z = 1{,}900$ at a typical spray voltage of 1.1 to 1.5 kV. Data were acquired with an FT MS resolution setting of 100,000 (at $m/z = 400$) and a linear ion trap target value of 1,000,000. MS spectra were deconvoluted to generate uncharged muropeptide masses using the QualBrowser program (ThermoElectron, Bremen, Germany).

**Online electrospray MS.** Online micro-HPLC–MS experiments were performed by injecting nonreduced muropeptide solutions (1 μl) onto a self-packed column (0.5 by 150 mm) of Reprosil-Pur $C_{18}$-AQ 3μ medium (Maisch, Ammerbuch, Germany) with a flow rate of 12 μl/min. The HPLC gradient was generated using an Agilent 1100 system with flow splitting (100 μl/min; split ratio, 1:10). The gradient conditions were 5 min with 0.5% buffer B (0.1% formic acid in acetonitrile) in buffer A (0.1% aqueous formic acid), followed by a 30 min gradient to 20% buffer B. Nonreduced muropeptides that eluted from the gradient column were analyzed by micro-HPLC–MS in positive ion mode using a Finnigan LTQ-FT FT mass spectrometer (ThermoElectron, Bremen, Germany) equipped with a Finnigan Nanospray ion source (ThermoElectron). Eluate was sprayed using uncoated TaperTips (inside diameter, 100-μm; New Objective, Woburn, MA) at a spray voltage of 2.25 kV. The mass spectrometer was used to perform survey MS scans over the mass range from $m/z = 300$ to $m/z = 1{,}500$ in data-dependent mode. MS data were acquired with an FT MS resolution setting of 100,000 (at $m/z = 400$) and a trap injection target value of 500,000. The top six ions in the parent scan were automatically subjected to MS-MS analysis in the linear ion trap region at a target value of 10,000. Mass spectrum plots and spectral deconvolution were generated using the QualBrowser program (ThermoElectron, Bremen, Germany).

**Determination of *meso*-$A_2$pm and LL-$A_2$pm.** Peptidoglycan from vegetative cells of *M. xanthus* was hydrolyzed with 4 M HCl at 100°C for 15 h. The hydrolysate was evaporated to dryness in a gentle air stream, and the residue was dissolved in 100 μl water and dried again. The dried material was redissolved in 50 μl water and analyzed by thin-layer chromatography on a cellulose plate using a previously described solvent system (38). Amino acids were stained using the ninhydrin reagent. A standard mixture containing *meso*-2,6-diaminopimelic acid (*meso*-$A_2$pm) and LL-diaminopimelic acid (LL-$A_2$pm) was included on the same plate, and the acids separated with the expected $R_f$ values (0.16 for *meso*-$A_2$pm and 0.22 for LL-$A_2$pm).

**Amino acid and amino sugar analysis.** Samples were hydrolyzed in 6 M HCl at 95°C for 16 h. After evaporation of the acid, the pellets were dissolved with 67 mM trisodium citrate-HCl buffer (pH 2.2) and injected into an Hitachi L8800 analyzer equipped with a 2620MSC-PS column (ScienceTec, Les Ulis, France). Amino acids and amino sugars were detected after postcolumn reaction with ninhydrin.

**TEM.** Cells were fixed with 2.5% paraformaldehyde, 0.2% glutaraldehyde, 30 mM sodium phosphate (pH 7.4) for 15 min at 20°C and for 30 min on ice. The cells were then sedimented, washed twice with phosphate-buffered saline, and resuspended in phosphate-buffered saline to an optical density of 1.0. For transmission electron microscopy (TEM), glutaraldehyde-fixed cells were embedded in 2% agarose and 1-mm blocks were cut out. After postfixation treatment with 1% osmium tetroxide in 100 mM phosphate buffer (pH 7.2) for 1 h on ice, the blocks were rinsed with double-distilled water, treated with 1% aqueous uranyl acetate for 1 h at 4°C, dehydrated using a graded ethanol series, and then embedded in Epon. Ultrathin sections were stained with uranyl acetate and lead citrate. Samples were viewed using a Philips CM10 electron microscope. Sacculi were visualized by TEM using a previously described protocol (8). Briefly, the sacculi were labeled on a grid with an affinity-purified antibody against peptidoglycan from *E. coli*. After washing, the preparation was incubated with a protein A—6-nm gold conjugate. After another washing procedure, the sacculi were contrasted with uranyl acetate and viewed with the Philips CM10 electron microscope.

**Estimation of the surface area of spore coats and of the surface densities of amino acids and amino sugars.** A sample of spore coats was placed on a microscope slide that was pretreated with 0.01% polylysine. After 2 min the remaining liquid was removed from the slide. Images were obtained by using the ×100 objective of a Zeiss Axiovert microscope and a Sony CoolSnap HQ cooled charge-coupled device camera (Roper Scientific Ltd.) attached to the microscope. Digital images were obtained with Metamorph (version 4.6.9) and were processed with ImageJ (version 1.38) to find the edges of the spore coats. The diameter of spore coats was measured by "straight-line selection." The surface area was calculated from the measured diameter by assuming that the spore coat was flat on the surface, and it was $9.87 \pm 1.81$ μm$^2$ ($n = 100$). The spore coat density in the sample was determined with a Thoma counting chamber (Weber, United Kingdom) using a Zeiss Axiovert microscope and a ×40 objective, and it was $4.37 \times 10^{11}$ spore coats per ml. The surface density of amino acids and amino sugars was estimated from the concentration of the compounds in a spore coat sample (as determined by amino acid and amino sugar analysis), the mean surface area of the spore coats, and the density of the spore coats in the sample.

## RESULTS

Muropeptides are the GlcNAc–*N*-acetylmuramic acid (MurNAc) disaccharide peptide building blocks of peptidoglycan released by treatment with a muramidase. They have characteristic, species-specific structural elements determined by the peptidoglycan biosynthetic pathway and the specificity of the enzymes involved. In all gram-negative bacteria studied thus far, the sequence of the pentapeptide is L-Ala–γ-D-Glu–*meso*-$A_2$pm–D-Ala–D-Ala (36, 40). Cross-linking and proteolytic reactions result in a high degree of structural diversity of muropeptides, which is reflected by the complex muropeptide pattern (or profile) of a given species. In addition to pentapeptides, the peptidoglycans of gram-negative bacteria contain variable amounts of the corresponding monomeric tetra-, tri- and dipeptides, as well as different types of dimeric, trimeric, and tetrameric (cross-linked) muropeptides. There are also particular structures marking the chain ends (1,6-anhydro-MurNAc-containing muropeptides) or the attachment sites of Braun's lipoprotein (muropeptides with a Lys-Arg dipeptide) (14, 15, 36).

***M. xanthus* has an unusual muropeptide profile.** Peptidoglycan was isolated from vegetative *M. xanthus* cells and from *E. coli* as described previously (14, 15). The material obtained was

TABLE 1. Molecular masses and ion current intensities of nonreduced muropeptides detected using micro-HPLC–LTQ-FT MS

| Muropeptide[a] | Theoretical neutral molecular mass (Da) | *M. xanthus* | | *E. coli* | |
|---|---|---|---|---|---|
| | | Neutral molecular mass (Da)[b] | Intensity (counts)[c] | Neutral molecular mass (Da)[b] | Intensity (counts)[c] |
| Di | 696.2702 | ND[d] | | 696.2697 | 2,217 |
| TriAnh | 850.3444 | ND | | 850.3449 | 1,131 |
| Tri | 868.3549 | ND | | 868.3541 | 11,424 |
| TetraAnh | 921.3815 | ND | | ND | |
| Tetra | 939.3921 | 939.3908 | 40,940 | 939.3907 | 116,440 |
| Penta | 1,010.4292 | 1,010.4295 | 17 | ND | |
| Tetra-X | 1,039.4081[e] | 1,039.4089 | 2,070 | ND | |
| TriLysArg | 1,152.5510 | ND | | 1,152.5502 | 3,050 |
| Tetra-Y | 1,311.5566[f] | 1,311.5567 | 281 | ND | |
| TriTri($A_2$pm) | 1,718.6993 | ND | | 1,718.6983 | 585 |
| TetraTriAnh | 1,771.7259 | ND | | 1,771.7257 | 958 |
| TetraTri | 1,789.7364 | ND | | 1,789.7348 | 14,224 |
| TetraTetraAnh | 1,842.7630 | 1,842.7627 | 4,896 | ND | |
| TetraTetra | 1,860.7736 | 1,860.7735 | 5,902 | 1,860.7721 | 33,434 |
| TetraPenta | 1,931.8107 | ND | | ND | |
| TetraTetraAnh-X | 1,942.7790[e] | 1,942.7781 | 671 | ND | |
| TriTri($A_2$pm)LysArg | 2,002.8954 | ND | | 2,002.8937 | 183 |
| TetraTriLysArgAnh | 2,055.9219 | ND | | 2,055.9157 | 18 |
| TetraTriLysArg | 2,073.9325 | ND | | 2,073.9311 | 1,285 |
| TetraTetraAnh-Y | 2,214.9275[f] | 2,214.9293 | 861 | ND | |
| TetraTetra-Y | 2,232.9381[f] | 2,232.9398 | 1,246 | ND | |
| TetraTetraTriAnh | 2,693.1074 | ND | | 2,693.1059 | 66 |
| TetraTetraTri | 2,711.1179 | ND | | 2,711.1,149 | 305 |
| TetraTetraTetradiAnh | 2,746.1339 | 2,746.1318 | 753 | ND | |
| TetraTetraTetraAnh | 2,764.1445 | 2,764.1453 | 1,673 | 2,764.1460 | 230 |
| TetraTetraTetra | 2,782.1550 | 2,782.1572 | 694 | 2,782.1,541 | 911 |
| TetraTetraTetraAnh-X | 2,864.1605[e] | 2,864.1564 | 232 | ND | |
| TetraTetraTriLysArgAnh | 2,978.3113 | ND | | ND | |
| TetraTetraTriLysArg | 2,995.3140 | ND | | ND | |
| TetraTetraTetraAnh-Y | 3,136.3090[f] | 3,136.3097 | 862 | ND | |
| TetraTetraTetra-Y | 3,154.3195[f] | 3,154.3200 | 183 | ND | |
| TetraTetraTetraTetradiAnh | 3,667.5154 | 3,667.5185 | 140 | ND | |
| TetraTetraTetraTetraAnh | 3,685.5260 | ND | | ND | |
| TetraTetraTetraTetra | 3,703.5365 | ND | | ND | |

[a] Muropeptides are designated as described by Glauner (14).
[b] Neutral molecular masses were calculated using the molecular masses of monocharged or multiply charged protonated compounds ($H^+$ form). Most compounds were also present in the $Na^+$ and $K^+$ forms.
[c] Intensities of the $H^+$ forms. The background signal was ~10 counts.
[d] ND, not detected.
[e] Molecular mass calculated by assuming that modification X is $C_4H_4O_3$.
[f] Molecular mass calculated by assuming that modification Y is Ala-Glu-$A_2$pm (without $H_2O$).

digested with the muramidase cellosyl to release the muropeptides. Nonreduced muropeptides were first analyzed by a newly developed, rapid method for detection in peptidoglycan digestion samples (see Materials and Methods). The muropeptide mixture was applied to a micro-$C_{18}$ reversed-phase HPLC column which was directly coupled to an LTQ-FT mass spectrometer. Ion peaks corresponding to the masses of expected muropeptides were identified in digests of the peptidoglycans from *M. xanthus* and *E. coli* (Table 1). With the exception of a few minor muropeptides, the masses of all previously described muropeptides of *E. coli* were identified by this method with high mass accuracy. We expected to obtain similar muropeptide profiles for *E. coli* and *M. xanthus*. Indeed, the *M. xanthus* sample contained several masses corresponding to the masses of muropeptides present in *E. coli*, including masses of the muropeptides Tetra, TetraTetra, TetraTetraAnh, TetraTetraTetra, and TetraTetraTetraAnh (see reference 15 for an explanation of the nomenclature of muropeptides). Comparison of MS-MS spectra of the major muropeptides of *M. xanthus* and *E. coli* revealed identical fragmentation products (not shown). In the *M. xanthus* sample the signals for anhydro (Anh) muropeptides which originated from glycan chain ends were generally greater. Also, the *M. xanthus* peptidoglycan masses included masses for additional anhydro muropeptides (TetraTetraTetradiAnh and TetraTetraTetraTetraAnh) not present in the *E. coli* sample, indicating that anhydro muropeptides might be more abundant in *M. xanthus* than in *E. coli*. The *M. xanthus* sample did not produce detectable mass signals for muropeptides with di- or tripeptides (for example, the muropeptide Di or Tri or the dimer TetraTri) or for muropeptides with the Lys-Arg modification originating from the covalently bound Braun's lipoprotein. On the other hand, the *M. xanthus* sample contained several molecules with masses corresponding to those of modified muropeptides. One modification (designated modification X [Table 1]) was present in the muropeptides Tetra, TetraTetraAnh, and TetraTetraTetraAnh and corresponded to a 100.02-Da increase in the molecular mass. Another modification (designated modification Y) was present

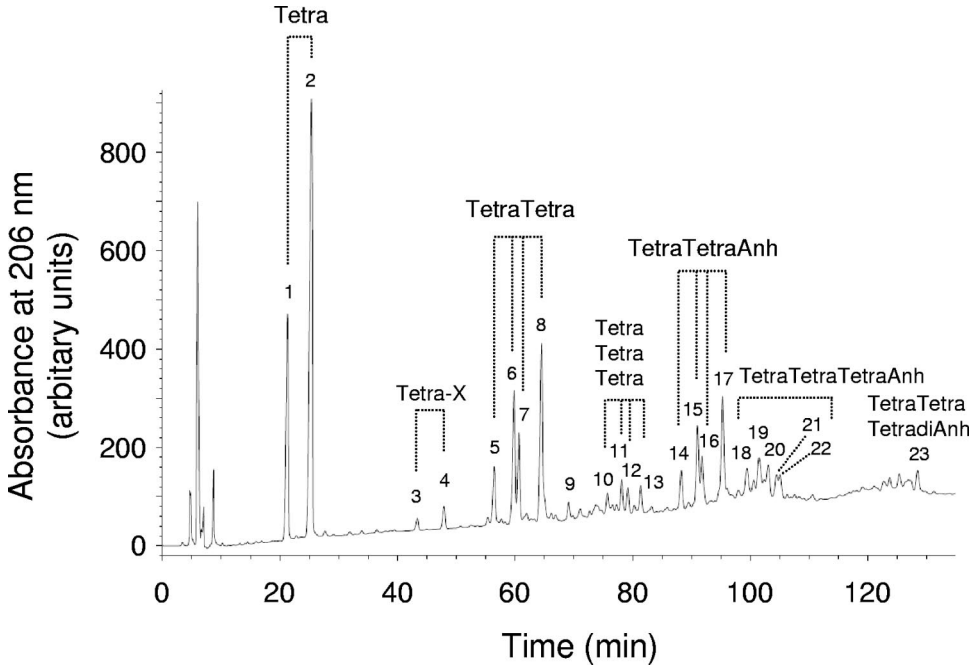


FIG. 1. Separation of muropeptides from *M. xanthus*. Muropeptides were released from peptidoglycan by cellosyl, reduced using sodium borohydride, and separated by $C_{18}$ reversed-phase HPLC. The numbers indicate fractions analyzed by LTQ-FT MS and correspond to the numbers of the muropeptides in Table 2 and Fig. 2. The names of the major muropeptides are indicated above the peaks, which illustrate the occurrence of muropeptide isomers resolved using HPLC.

in the muropeptides Tetra, TetraTetraAnh, TetraTetra, Tetra-TetraTetraAnh, and TetraTetraTetra and increased the molecular masses of these molecules by 372.16 Da. Overall, micro-HPLC–LTQ-FT MS analysis revealed remarkable differences in the muropeptide profiles of *M. xanthus* and *E. coli*. We also analyzed the muropeptide composition of *M. xanthus* by using classical HPLC separation and offline electrospray MS.

**Muropeptide composition of *M. xanthus*: presence of *meso*-$A_2$pm and LL-$A_2$pm.** Muropeptides of *M. xanthus* were reduced with sodium borohydride and separated by $C_{18}$ reversed-phase HPLC using a method described previously for *E. coli* muropeptides (14, 15). More than 20 muropeptides were separated. The peak pattern was strikingly different from the previously described pattern obtained for *E. coli* muropeptides (Fig. 1 and Table 2) (14, 15). Twenty-three muropeptide fractions were collected, concentrated, desalted, and analyzed by LTQ-FT MS (Table 2). None of the major components in the monomeric region of the chromatogram corresponded to the muropeptide Di, Tri, or Penta, which was consistent with the results obtained by micro-HPLC–LTQ-FT MS. Surprisingly, both major monomeric muropeptide peaks (Fig. 1, peaks 1 and 2) had the expected molecular mass of the muropeptide Tetra, as determined by LTQ-FT MS with molecular mass accuracy in the low range (<5 ppm). The muropeptide Tetra of *E. coli* coeluted with muropeptide 2 of *M. xanthus*, but no *E. coli* muropeptide coeluted with muropeptide 1 of *M. xanthus* (not shown). Moreover, the *M. xanthus* sample contained four dimers (muropeptides 5, 6, 7, and 8) with the expected molecular mass of TetraTetra, and one of them (muropeptide 6) coeluted with *E. coli* TetraTetra (not shown). *M. xanthus* had also four dimers (muropeptides 14, 15, 16, and 17) with the expected molecular mass of TetraTetraAnh and several trimers with the molecular mass of TetraTetraTetra or Tetra-TetraTetraAnh. From these results we inferred that the basic building blocks in the peptidoglycan of *M. xanthus* exist in two versions with the same molecular mass; i.e., there are two isomers of monomers, four isomers of dimers, and (theoretically) eight isomers of trimers. The isomeric monomers and dimers could be separated using the HPLC conditions described here. The presence of such muropeptide isomers in a single species has not been described previously.

In order to determine the structural basis for the observed muropeptide isomerization, a sample of *M. xanthus* peptidoglycan was hydrolyzed with hydrochloric acid, and the resulting amino sugar-amino acid mixture was analyzed by thin-layer chromatography. This method is routinely used for peptidoglycan analysis during characterization of bacterial taxa at the German Collection of Microorganisms and Cell Cultures. Interestingly, myxococcal peptidoglycan contained both *meso*-$A_2$pm and LL-$A_2$pm at a molecular ratio of about 1 to 0.4. The presence of two $A_2$pm isomers in *M. xanthus* was unexpected because only *meso*-$A_2$pm has been found in the peptidoglycan of all other gram-negative bacteria studied thus far (36, 40). This would explain the pattern of muropeptide isomers observed. We inferred that muropeptide 1 (Fig. 1) is the muropeptide Tetra containing LL-$A_2$pm, whereas muropeptide 2 is the "normal" Tetra muropeptide with *meso*-$A_2$pm (hence, muropeptide 2 coeluted with *meso*-$A_2$pm-containing Tetra of *E. coli*). Also, the observed peak ratio of muropeptide 2 to muropeptide 1 was approximately the same as the measured ratio of *meso*-$A_2$pm to LL-$A_2$pm in the peptidoglycan. We suggest the following structures for the four isomers of the

TABLE 2. Reduced muropeptides detected in HPLC fractions

| Compound (muropeptide)[a] | Proposed structure | Retention time (min) | Relative peak area (%) | Neutral molecular mass (Da) of reduced compound (HPLC fractions) | |
|---|---|---|---|---|---|
| | | | | Calculated | Determined |
| 1 | Tetra$^{LL}$ | 21.3 | 9.3 | 941.4077 | 941.4071 |
| 2 | Tetra$^{meso}$ | 25.4 | 22.9 | 941.4077 | 941.4051 |
| 3 | Tetra-X$^{LL}$ | 43.4 | 0.5 | 1,041.4238[b] | 1,041.4208 |
| 4 | Tetra-X$^{meso}$ | 47.9 | 1.0 | 1,041.4238[b] | 1,041.4208 |
| 5 | TetraTetra$^{LL/LL}$ | 56.5 | 2.7 | 1,864.8049 | 1,864.8039 |
| 6 | TetraTetra$^{meso/meso}$ | 59.8 | 6.2 | 1,864.8049 | 1,864.8028 |
| 7 | TetraTetra$^{meso/LL}$ | 60.6 | 3.9 | 1,864.8049 | 1,864.8038 |
| 8 | TetraTetra$^{LL/meso}$ | 64.5 | 8.9 | 1,864.8049 | 1,864.8031 |
| 9 | TetraTetra-Y | 69.1 | 0.7 | 2,236.9694[c] | 2,236.9660 |
| 10 | TetraTetraTetra | 75.7 | 1.2 | 2,788.2020 | 2,788.1977 |
| 11A | TetraTetraTetra | 78.1 | 1.6 | 2,788.2020 | 2,788.1951 |
| 12 | TetraTetraTetra | 79.2 | 1.2 | 2,788.2020 | 2,788.1997 |
| 13 | TetraTetraTetra | 81.4 | 1.3 | 2,788.2020 | 2,788.1988 |
| 14 | TetraTetraAnh | 88.3 | 1.8 | 1,844.7786 | 1,844.7770 |
| 15 | TetraTetraAnh | 91.0 | 3.8 | 1,844.7786 | 1,844.7775 |
| 16 | TetraTetraAnh | 91.8 | 2.4 | 1,844.7786 | 1,844.7776 |
| 17 | TetraTetraAnh | 95.3 | 5.3 | 1,844.7786 | 1,844.7784 |
| 18A | TetraTetraTetraAnh | 99.4 | 2.1 | 2,768.1758 | 2,768.1753 |
| 19A | TetraTetraTetraAnh | 101.5 | 2.9 | 2,768.1758 | 2,768.1753 |
| 20A | TetraTetraTetraAnh | 103.0 | 2.0 | 2,768.1758 | 2,768.1743 |
| 21 | TetraTetraTetraAnh | 104.4 | 1.3 | 2,768.1758 | 2,768.1762 |
| 22 | TetraTetraTetraAnh | 105.0 | 1.4 | 2,768.1758 | 2,768.1767 |
| 23 | TetraTetraTetra(diAnh) | 128.4 | 1.0 | 2,748.1496 | 2,748.1515 |
| 11B | TetraTetra-X | 78.1 | ND[d] | 1,964.8209[b] | 1,964.8174 |
| 18B | TetraTetraTetraAnh-Y | 99.4 | ND[e] | 3,140.3403[c] | 3,140.3383 |
| 19B | TetraTetraTetraAnh-Y | 101.5 | ND[f] | 3,140.3403[c] | 3,140.3393 |
| 20B | TetraTetraTetraAnh-Y | 103.0 | ND[g] | 3,140.3403[c] | 3,140.3406 |
| 20C | TetraTetraAnh-X | 103.0 | ND[g] | 1,944.7947[b] | 1,944.7937 |

[a] The numbers correspond to peak numbers in Fig. 1.
[b] Molecular mass calculated by assuming that modification X is $C_4H_4O_3$.
[c] Molecular mass calculated by assuming that modification Y is Ala-Glu-$A_2$pm (without $H_2O$).
[d] ND, not detected. Minor component that coelutes with 11A.
[e] Minor component that coelutes with 18A.
[f] Minor component that coelutes with 19A.
[g] Minor component that coelutes with 20A.

major dimeric muropeptide (TetraTetra) based on their abundance and elution behavior. Compound 6 coeluted with TetraTetra of *E. coli* and is most likely the "normal" version with two *meso*-$A_2$pm residues. Compound 5 eluted earlier than compounds 6, 7, and 8, and its abundance was lowest; therefore, it is most likely the isomer with two LL-$A_2$pm residues. Compounds 7 and 8 presumably contain one *meso*-$A_2$pm residue and one LL-$A_2$pm residue (Table 2 and Fig. 2). The four TetraTetraAnh isomers (muropeptides 14 to 17) gave rise to a peak pattern in the chromatogram similar to that produced by the TetraTetra isomers and are likely to have an analogous $A_2$pm profile.

The average length of the glycan strands could be estimated from the fraction of anhydro-MurNAc residues. The glycan strands were relatively short in *M. xanthus*, and the average length was 8.9 disaccharide units (calculated using muropeptides 1 to 23). This value is, if anything, an overestimate because some of the unidentified, minor muropeptides with high retention times were likely to carry an anhydro group. Although the fraction of anhydro-muropeptides was high, we found that all detectable anhydro groups were present in oligomeric structures (dimers to tetramers), and we could not detect the monomeric molecule TetraAnh. Thus, the majority (if not all) of the anhydro ends of the glycan strands are connected to other strands by peptide cross-links. About 60.4% of the peptides in the myxococcal peptidoglycan were present in cross-links, and a relatively high proportion (18.7%) were present in trimeric structures.

**Nature of the modifications in the myxococcal peptidoglycan.** We identified by using MS two modifications in the myxococcal peptidoglycan, both of which are low-abundance modifications. The X modification was present in about 4.5% of all monomers, and the Y modification (present in muropeptide 9) accounted for about 0.7% of the total UV-absorbable material and was also present in several minor muropeptides (muropeptides 18B, 19B, and 20B) that coeluted with the TetraTetraTetraAnh isomers. Such modifications to the muropeptide structure might occur by proteolytic cleavage or by addition of a structural element. The molecular mass of the Y modification (372.1645 Da) coincided exactly with the theoretical molecular mass of a Glu-$A_2$pm-Ala tripeptide without water (372.16450 Da). MS-MS analysis of protonated muropeptide 9 showed that there was initial loss of the GlcNAc residues, which is generally observed with muropeptides. Both Glu and Ala could be lost from the resulting fragment (muropeptide 9 lacking GlcNAc) (data not shown). This was expected based on the proposed structure of muropeptide 9 with a terminal Glu residue and was not seen with muropeptides with Glu in a

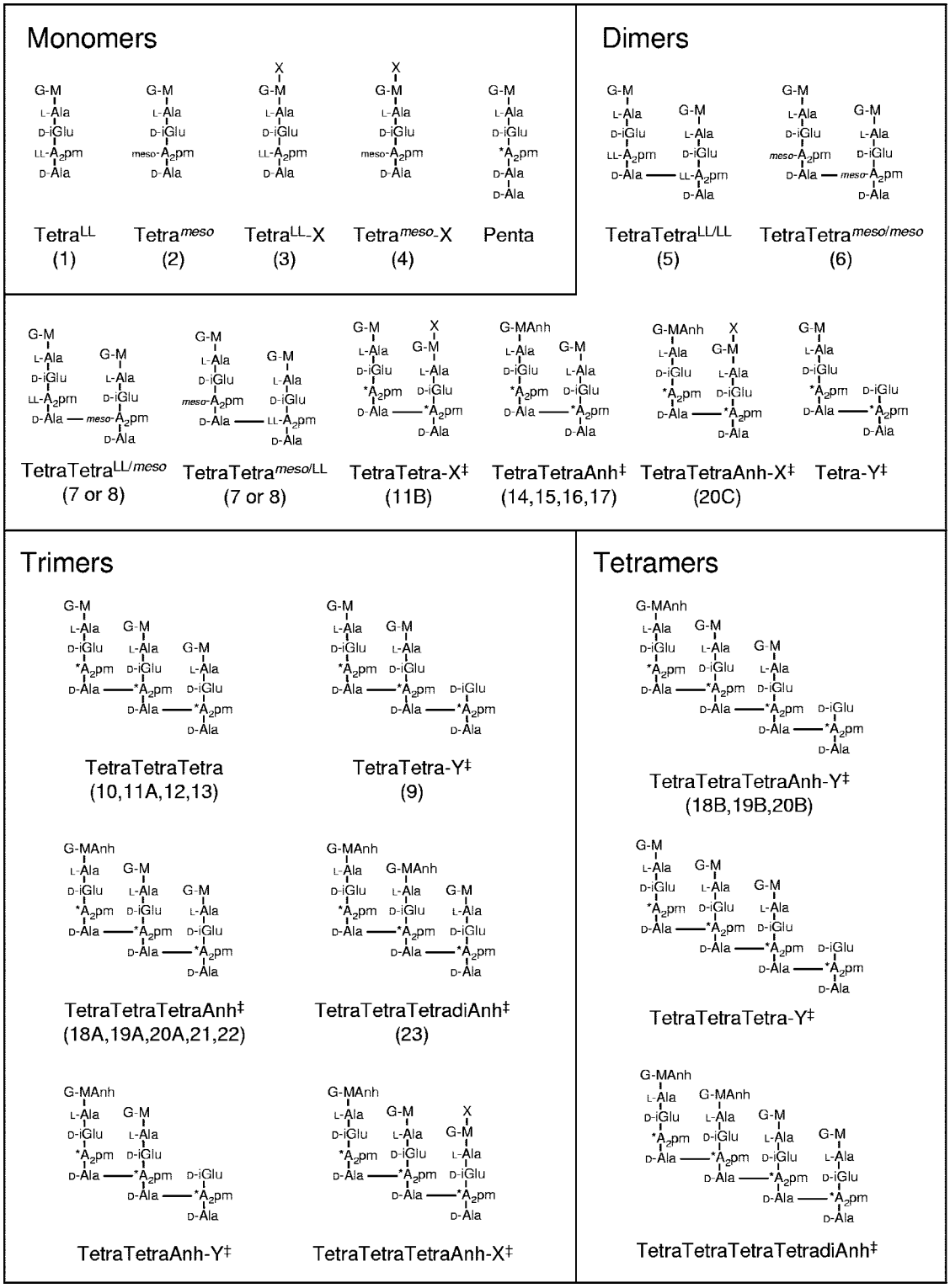


FIG. 2. Proposed structures of the muropeptides from *M. xanthus*. The numbers correspond to the peak numbers in Fig. 1. Minor compounds without numbers were detected only by micro-HPLC–LTQ-FT MS analysis. ∗$A_2$pm, either *meso*-$A_2$pm or LL-$A_2$pm. A double dagger indicates that the position of the modification (Anh, X, or Y) is not known. For example, for some structures it is not known which of the MurNAc residues carries the Anh or X modification.

peptide chain. Thus, it is most likely that compounds with the Y modification were formed from an oligomeric muropeptide by proteolytic cleavage between L-Ala and D-Glu by an LD-endopeptidase, resulting in release of the GlcNAc–MurNAc–L-Ala moiety.

Two isomeric monomers (muropeptides 3 and 4) contained the X modification. The exact molecular mass of modification X was determined by subtracting the molecular masses of the unmodified muropeptides from the molecular masses of the modification X-containing muropeptides in LTQ-FT MS experiments performed with mixtures of nonreduced samples and was found to be 100.0173 ± 0.0011 Da. Based on the accuracy of the molecular mass determined, only one elemental composition of modification X appears to be possible: $C_4H_4O_3$ (theoretical molecular mass, 100.016045 Da). Other possible combinations of C, N, O, and H atoms result in theoretical molecular masses which do not fit the observed molecular mass difference given the mass accuracy. Also, the observed isotope profile of modification X-containing muropeptides excluded the possibility of the presence of other atoms, such as S or P. Incubation of peptidoglycan with 80 mM sodium hydroxide for 1 h resulted in the absence of any detectable muropeptides with modification X, while all other muropeptides could be detected, indicating that muropeptides with modification X are alkali labile (not shown). However, several attempts to identify the H-X-OH compound in the supernatant of NaOH-treated sacculi by electron impact MS failed, possibly because of the small amounts of material obtained.

The MS-MS data allowed identification of the attachment site of modification X in the muropeptide Tetra. (i) Fragmentation of Tetra-X, fragmentation of *M. xanthus* Tetra, and fragmentation of *E. coli* Tetra all gave rise to a strong molecular mass signal at 534.2 Da, which corresponded to the protonated lactyl-tetrapeptide moiety. MS-MS-MS analysis of the 534.2-Da ions present in the fragmented Tetra-X or Tetra sample revealed identical fragmentation patterns. Further, fragmentation of all three compounds resulted in a positive ion with a molecular mass of 719.2 Da corresponding to the protonated and dehydrated MurNAc-tetrapeptide ion. Thus, Tetra-X has an unmodified peptide and peptide-MurNAc linkage, and modification X must be attached to either GlcNAc or MurNAc (or both). (ii) Both GlcNAc and modification X were readily lost in fragmentation experiments with protonated Tetra-X (1,040.4 Da), resulting in fragments corresponding to the loss of GlcNAc (a loss of 203.1 Da) or modification X (a loss of 100.0 Da) or both (a loss of 303.1 Da). (iii) MS-MS-MS analysis of the weak signal of the protonated Tetra-X(-GlcNAc) ion (837 Da) revealed loss of modification X (a loss of 101 Da). From these results we concluded that modification X must be attached to the MurNAc residue. It was possible to reduce Tetra-X with sodium borohydride, which resulted in a 2-Da increase in the molecular mass. Reduction requires the presence of a free OH group at the anomeric C-1 position of MurNAc, thereby excluding the possibility that modification X is attached there. Because there are no free OH groups at positions 2, 3, 4, and 5 of MurNAc, the only remaining possible position for the attachment of modification X is the C-6 OH. We therefore concluded that modification X is most likely attached to the C-6 OH of MurNAc by an alkali-labile ester bond.

**Visualization of sacculi from vegetative cells and myxospores.** Vegetative cells of *M. xanthus* were harvested, and peptidoglycan sacculi were prepared for TEM by repeated incubation in hot SDS and treatment with protease to remove contaminating proteins. The material obtained was immobilized on grids and contrasted with uranyl acetate. TEM revealed the presence of typical sacculi whose sizes were similar to those of *M. xanthus* cells. The sacculi from *M. xanthus* were incubated on a grid with an antibody raised against peptidoglycan from *E. coli* and then with a protein A—6-nm gold conjugate. Examination of the samples by TEM revealed that the *M. xanthus* sacculi were uniformly labeled with gold particles (Fig. 3A). These results indicate that vegetative cells of *M. xanthus* have a continuous peptidoglycan sacculus with structural elements similar to the structural elements of the peptidoglycan of *E. coli*, which is in agreement with the results of the muropeptide analysis described here.

We attempted to visualize the sacculi from both myxospores and cells in the transition from the vegetative form to the spore form using TEM. We confirmed the previous observation that rod-shaped, vegetative cells of *M. xanthus* changed to spherical myxospores within 2.5 to 3 h during cultivation in the presence of 0.5 M glycerol in aerated liquid medium. Under these conditions, conversion to myxospores was almost quantitative, as judged from microscopic examination of the cells. Sacculi from sporulating cells or from myxospores were isolated in the same way as sacculi from vegetative cells, immobilized on grids, immunolabeled with anti-peptidoglycan antibody–protein A—6-nm gold conjugate, contrasted with uranyl acetate, and examined by TEM. Spore sacculi were spherical and bag-shaped objects whose electron density differed from that of sacculi isolated from vegetative cells (Fig. 3C). These spore sacculi contained areas with very high electron density. They appeared to consist of the same material as the myxospore coats described previously (21) and were not labeled by the anti-peptidoglycan antiserum. Moreover, incubation of spore coats with cellosyl did not result in release of muropeptides; HPLC analysis of a sample failed to detect muropeptides or any other UV-absorbable material in the supernatant of the cellosyl digest even when the spore coats were mechanically broken using glass beads prior to cellosyl digestion (not shown). Samples from cells in transition from vegetative cells to spores contained both bag-shaped spore coats not labeled by anti-peptidoglycan antiserum and peptidoglycan patches of various sizes labeled with the antibody (Fig. 3B). Frequently one or more patches of peptidoglycan were attached to a spherical spore coat, indicating that they could have originated from the same cell. These results show that development into myxospores involves both formation of a new spore coat, which does not consist of peptidoglycan, and degradation of the rod-shaped peptidoglycan sacculus.

**Do the glycerol-induced myxospores contain a peptidoglycan sacculus?** Our failure to detect muropeptides in the spore coats could have been due to different factors. Either the spore coat did not contain a significant amount of peptidoglycan, or it contained peptidoglycan which could not be degraded by muramidase or recognized by the antiserum. To determine if the spore coat contained peptidoglycan, we hydrolyzed the

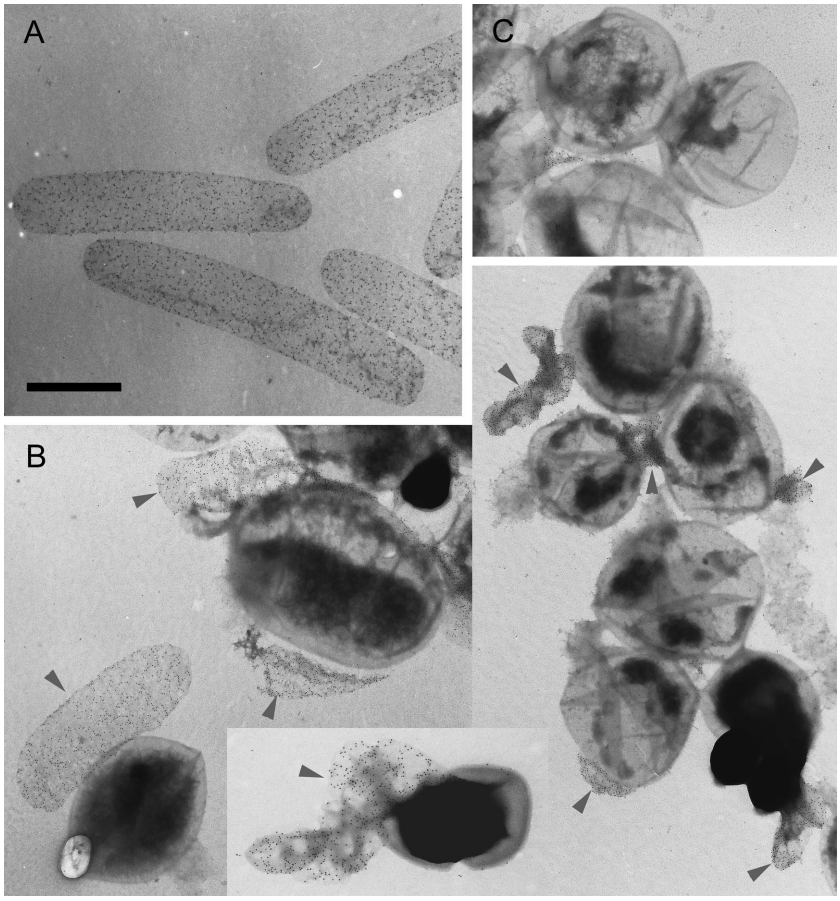


FIG. 3. TEM of sacculi from *M. xanthus*. Sacculi from (A) vegetative cells, (B) sporulating cells, and (C) myxospores were immobilized on a grid and incubated with anti-peptidoglycan antibody, followed by 6-nm gold-labeled protein A. After washing, the sacculi were contrasted with uranyl acetate. Gold particles are indicated by small dots. Sacculi of vegetative cells were rod shaped and were recognized by the anti-peptidoglycan antibody, in contrast to the spherical sacculi of myxospores, which were not labeled. Sporulating cells had unlabeled spherical sacculi with attached pieces of labeled peptidoglycan of various sizes (arrowheads). Bar = 1 μm (for all images).

material, quantified the amino acids and amino sugars, and related the amounts of these compounds to the surface area of spore coats. Isolated spore coats had an average surface area of 9.87 ± 1.81 $\mu m^2$ ($n$ = 100) as determined by light microscopy (see Materials and Methods). Table 3 shows the compounds identified and the amount per unit of surface area. The spore coat material contained variable amounts of all of the amino acids present in proteins. Glycine, alanine, and glutamic acid were the most abundant amino acids. The spore coats also contained glucosamine and small amounts of $A_2$pm and muramic acid. Because the latter two compounds are present only in peptidoglycan, it is likely that the spore coats contained a small amount of peptidoglycan.

The new spore coat layer could be observed in thin sections of glutaraldehyde-fixed spores prepared and visualized by TEM. Both vegetative cells and spores contained an inner cell membrane and an outer cell membrane separated by periplasmic space (Fig. 4). The resolution and contrast of the electron micrographs were not high enough to recognize the peptidoglycan layer. The spores had extra membrane loops and membrane vesicles on the surface, presumably because the surface area-to-volume ratio decreased during the transition

TABLE 3. Surface densities of amino acids and amino sugars in glycerol spore coats

| Amino acid or amino sugar | Surface density ($10^{10}$ nmol/$\mu m^2$)[a] |
|---|---|
| Ala | 20.3 ± 0.3 |
| Arg | 8.12 ± 0.13 |
| $A_2$pm | 0.52 ± 0.01 |
| Asp | 13.4 ± 0.1 |
| Cys | 0.18 ± 0.02 |
| GlcN | 3.54 ± 0.09 |
| Glu | 17.8 ± 0.3 |
| Gly | 28.7 ± 0.2 |
| His | 2.57 ± 0.05 |
| Ile | 5.05 ± 0.12 |
| Leu | 13.1 ± 0.2 |
| Lys | 8.57 ± 0.10 |
| Met | 0.56 ± 0.06 |
| Mur | 1.40 ± 0.04 |
| Phe | 4.93 ± 0.07 |
| Pro | 7.65 ± 0.09 |
| Ser | 9.36 ± 0.13 |
| Thr | 7.84 ± 0.14 |
| Tyr | 3.27 ± 0.07 |
| Val | 6.77 ± 0.11 |

[a] The values are means ± standard deviations obtained from analyses of three different hydrolysates.

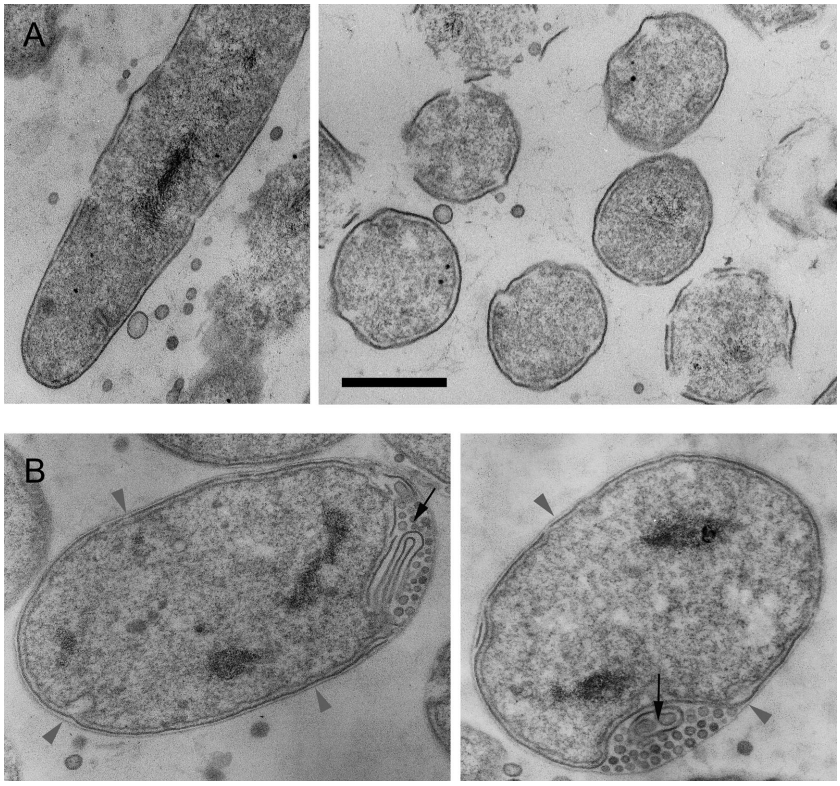


FIG. 4. TEM of thin sections of *M. xanthus*. (A) Thin section of a vegetative cell (side view) (left panel) or several vegetative cells cut perpendicular to the long axis (right panel). (B) Thin sections through myxospores, showing the presence of an additional outer layer (arrowheads) surrounding the outer membrane and encasing regions with accumulated membrane bends and vesicles (arrows). Bar = 1 μm (for all images).

from the rod shape to the spherical shape and thus the cells accumulated extra membrane. A thin spore coat layer surrounded the outer membrane and the extra membrane material of the spores (Fig. 4B).

## DISCUSSION

The presence of a *meso*-$A_2$pm residue at position 3 of the stem peptide has been the hallmark of the peptidoglycan of gram-negative bacteria and of some gram-positive species (for example, *Bacillus subtilis*) (46). In this work we found that in *M. xanthus* peptidoglycan a significant fraction (about 30%) of the stem peptides had an LL-$A_2$pm residue in place of the "normal" *meso*-$A_2$pm residue. LL-$A_2$pm has been detected in the peptidoglycans of several gram-positive species, including *Streptomyces* spp. and members of the families *Propionibacteriaceae* and *Intrasporangiaceae* (40). The occurrence of LL-$A_2$pm in combination with *meso*-$A_2$pm has been found in species of the actinomycete *Kitasatosporia*, where LL-$A_2$pm was found in the aerial mycelium and *meso*-$A_2$pm was found in the vegetative mycelium of the same strain (43). LL-$A_2$pm has not been described as a component of peptidoglycan in any gram-negative species. Also, LL-$A_2$pm is not present in the peptidoglycan of an unclassified member of the *Myxococcales*, *Myxobacter* sp. strain AL-1 (16). There are three slightly different bacterial pathways for the synthesis of *meso*-$A_2$pm, which is also a precursor of L-lysine (5, 50). Sequence comparisons revealed that *M. xanthus* strain DK1622 contains homologues of all four genes (*dapC*, *dapD*, *dapE*, and *dapF*) of the succinylase pathway, in which LL-$A_2$pm is the direct precursor of *meso*-$A_2$pm. Therefore, it is possible that *M. xanthus* has cytoplasmic pools of both LL-$A_2$pm and *meso*-$A_2$pm. The amino acid ligase MurE is responsible for addition of the third amino acid (most often a diamino acid) to the peptidoglycan precursor UDP–MurNAc–L-Ala–D-Glu. In most cases MurE exhibits high specificity for its amino acid. This has been shown for the *meso*-$A_2$pm-adding enzyme from *E. coli* and the L-Lys-adding enzyme from *Staphylococcus aureus* (3). However, sometimes MurE appears to lose its strict specificity. The peptidoglycan of some species of *Bifidobacterium* contains both L-Lys and L-Orn at position 3 (40). Another example is MurE from *Thermatoga maritima*, which can add L-Lys and D-Lys with comparable efficiencies (4). The genome of *M. xanthus* DK1622 contains a single *murE* homologue (accession number NC_008095). Presumably, this myxococcal MurE is capable of adding both *meso*-$A_2$pm and LL-$A_2$pm to the peptidoglycan precursor.

In *M. xanthus* all the peptidoglycan biosynthetic steps following the MurE step appear to function with both *meso*-$A_2$pm- and LL-$A_2$pm-containing peptides, resulting in the variety of muropeptide structures demonstrated here. It is quite remarkable that both the LL-$A_2$pm- and *meso*-$A_2$pm-containing peptides can participate in cross-linking reactions, as shown by the presence of all four possible isomers of the dimeric muropeptides. Cross-linking reactions are catalyzed by a set of acyl serine transferases (the penicillin-binding proteins [PBPs]), which form a new peptide bond between the tetrapep-

tidyl residue of a donor peptide and the ε-amino group of the $A_2$pm residue of an acceptor peptide. Either the PBPs of *M. xanthus* are generally nonspecific with respect to the configuration of $A_2$pm, or there are separate PBPs specific for LL-$A_2$pm-containing peptides and for *meso*-$A_2$pm peptides. The presence of LL-$A_2$pm could also have implications for the activity of peptidoglycan endopeptidases cleaving the peptide cross-links.

Although we have determined the likely sum formula ($C_4H_4O_3$) of modification X, our attempts to establish the chemical structure of this molecule were not sucessful because of the low abundance of the modified muropeptides, which made it impossible to obtain amounts sufficient for nuclear magnetic resonance analysis. However, there may be other myxococcal strains or bacterial species containing larger amounts of muropeptides with modification X that are sufficient for nuclear magnetic resonance analysis. The structure of modification X differs from the structures of previously described modifications in glycan strands (45), but, like the frequently found O-acetyl or phosphate groups, modification X is most likely attached to the C-6 OH of MurNAc. Possible biological compounds consistent with $C_4H_6O_4$, the sum formula of H-X-OH, are succinic acid and methylmalonic acid. We also identified several minor muropeptides with the Y modification. These muropeptides appear to be degradation products resulting from cleavage by an endopeptidase between L-Ala and $A_2$pm. Although enzymes with this specificity are present in other bacteria (48), the peptidoglycan endopeptidase of *M. xanthus* responsible for producing such muropeptides with modification Y has yet to be identified.

The peptidoglycan of *M. xanthus* has relatively short glycan strands; the average length is about 9 disaccharide units, which is significantly less than the average length of glycan strands reported for *E. coli* (21 to 35 disaccharide units) (14, 17, 47). The presence of shorter glycan strands in *M. xanthus* might be compensated for by increased peptide cross-linkage, which occurs to a greater degree in *M. xanthus* than in *E. coli*. In contrast to *E. coli*, in *M. xanthus* all detectable glycan chain ends were at cross-linked peptides (and not at monomeric, non-cross-linked peptides), which might be an important structural feature of peptidoglycan containing short glycan strands. Other species with relatively short glycan strands are the gram-negative organism *Helicobacter pylori* (6, 7) and the gram-positive organism *S. aureus* (2). Other remarkable features of the peptidoglycan from *M. xanthus* are the absence of detectable amounts of tripeptides and the low levels of pentapeptides. In *M. xanthus* pentapeptides are almost quantitatively cleaved to tetrapeptides by DD-carboxypeptidase(s), whereas the tripeptide-producing LD-carboxypeptidases are either not present or poorly active. Significant (and variable) amounts of tripeptides are present in the peptidoglycans of many gram-negative bacteria (36). In addition to *M. xanthus*, *Caulobacter crescentus* is gram-negative species with very low levels of tripeptides (26). Unlike the situation in *M. xanthus*, in *C. crescentus* there are significantly increased amounts of pentapeptides in the peptidoglycan. Whether the relative amounts of tri-, tetra-, and pentapeptides are important for specific physiological features in *M. xanthus* and other species is not known, but in *E. coli* trimming of pentapeptides to tetrapeptides by DD-carboxypeptidases is required to maintain the normal rod shape under certain conditions (9, 28, 44).

A previous study reported that sacculi of vegetative *M. xanthus* cells disintegrate upon treatment with hot detergent (SDS) and protease, suggesting that there is a discontinuous layer (52). We could not confirm these observations. We observed intact peptidoglycan sacculi of *M. xanthus* using electron microscopy (Fig. 3). These sacculi remained intact after incubation with 4% SDS (4 h at 95°C or 18 h at 80°C) and with different proteases (chymotrypsin or pronase; incubation for 12 h at 37°C) (not shown). It is possible that the sacculi used in the previous study were contaminated with one or more endogenous peptidoglycan hydrolases. High numbers of these autolysins are known to be present in *M. xanthus* (41). For preparation of our sacculi we paid particular attention to rapidly and quantitatively inactivating the autolysins by dropping the ice-cold cell suspension of *M. xanthus* cells into a boiling SDS solution, followed by repeated boiling steps in an SDS solution to remove attached proteins.

One of our initial goals was to establish the structure of the peptidoglycan in myxospores. This could be done only with glycerol-induced myxospores obtained in liquid culture, because the amount of pure spores that could be isolated from fruiting bodies was too small for peptidoglycan preparation and analysis. We realize that glycerol-induced myxospores differ in several ways from myxospores formed naturally in fruiting bodies. An important difference is the absence in glycerol-induced myxospores of surface protein S, which is synthesized during development of the fruiting body and which is the major component of the thick spore coat (18). Glycerol-induced myxospores form a thinner polysaccharide spore coat containing 14% protein, 8% glycine, and less than 1% organic phosphorus (21). In electron micrographs the appearance of the spore coats isolated in this work (Fig. 3C) and the appearance of the spore coats described previously (21) are similar. Although the isolation procedures were not identical, the different spore coat samples appeared to originate from the same layer surrounding the outer membrane of the glycerol spores (Fig. 3C).

It is not known from the literature whether myxospores contain peptidoglycan. To our surprise, we found that glycerol-induced myxospores do not contain a detectable amount of muropeptides. We first reasoned that the muramidase cellosyl might not be able to access the peptidoglycan because it is shielded by the spore coat. However, there was no release of muropeptides by cellosyl even after the spore coats were mechanically broken with glass beads (not shown), eliminating the possibility that there is shielding effect. Electron microscopy showed that spore coats were not recognized by antiserum against peptidoglycan, whereas patches of peptidoglycan were present on spore coats in a sample from cells which were in the process of glycerol-induced sporulation. These observations established that the peptidoglycan sacculus is degraded during glycerol-induced sporulation. Nonetheless, the spore coats contained small amounts of *N*-acetylmuramic acid and diaminopimelic acid, suggesting that they contained some peptidoglycan. The surface densities of *meso*-$A_2$pm and muramic acid in spore coats ($0.52 \times 10^{10}$ and $1.40 \times 10^{10}$ nmol/μm$^2$, respectively [Table 3]) are significantly lower than the reported surface density of *meso*-$A_2$pm in *E. coli* ($7.0 \times 10^{10}$ nmol/μm$^2$; calculated from the average number of *meso*-$A_2$pm molecules

per cell and the average cell surface area [53]). Considering that the amount of peptidoglycan in *E. coli* can form at most two complete layers (24, 35, 53), the glycerol spore coats from *M. xanthus* cannot have a complete layer of peptidoglycan. There are several possible explanations for the observed small amount of peptidoglycan in glycerol spores: (i) some peptidoglycan fragments were retained in the coats after degradation of the sacculus; (ii) parts of the sacculus were not degraded during glycerol-induced sporulation; or (iii) the residual peptidoglycan originated from a small fraction of cells which did not sporulate or which started but did not complete the sporulation process.

From this work we concluded that glycerol-induced myxospore development includes synthesis of a new spore coat and degradation of most if not all of the peptidoglycan sacculus. This is in sharp contrast to the formation of endospores in gram-positive bacteria, such as *B. subtilis* or *Clostridium sporogenes*. Although these species degrade the peptidoglycan of the mother cell, they retain a structurally modified peptidoglycan sacculus around the spore (33, 34). Also, streptomycetes keep their peptidoglycan during development from aerial hyphae to spore chains (29). It remains to be established whether myxospores developing in a fruiting body retain peptidoglycan and whether glycerol-induced myxospores rebuild a peptidoglycan sacculus once they age.

The absence of a peptidoglycan sacculus implies that in glycerol-induced myxospores the spore coat is responsible for osmotic stability, a function which is consistent with the bag shape and the size of isolated spore coats shown in this and previous work (21). The molecular architecture of the spore coat is not known. It is possible that, like peptidoglycan, the spore coat forms a single netlike (or cross-linked) macromolecule able to withstand the spore's turgor. Other interesting questions arising from this work are, how is the synthesis of the spore coat coordinated with the degradation of the peptidoglycan sacculus during spore formation and how is the rod-shaped peptidoglycan sacculus resynthesized during germination.

## ACKNOWLEDGMENTS

We thank Miguel de Pedro of Universidad Autónoma de Madrid, Madrid, Spain, for providing anti-peptidoglycan antibody and technical advice; Dave Dunbar of the Chemical Analysis Services Unit, Newcastle University, Newcastle upon Tyne, United Kingdom, for performing the electron impact MS analysis; and Richard Daniel of Newcastle University for technical advice concerning determination of the surface area of the spore coats.

This work was supported by the European Commission through the EUR-INTAFAR project (grant LSHM-CT-2004-512138).

## REFERENCES

1. **Bacon, K., and E. Rosenberg.** 1967. Ribonucleic acid synthesis during morphogenesis in *Myxococcus xanthus*. J. Bacteriol. **94:**1883–1889.
2. **Boneca, I. G., Z. H. Huang, D. A. Gage, and A. Tomasz.** 2000. Characterization of *Staphylococcus aureus* cell wall glycan strands, evidence for a new beta-*N*-acetylglucosaminidase activity. J. Biol. Chem. **275:**9910–9918.
3. **Boniface, A.** 2007. Etude des relations structure-activité au sein de la famille des Mur synthétases, enzymes de la voie de biosynthèse du peptidoglycane. Ph.D. thesis. Université Paris-Sud, Orsay, France.
4. **Boniface, A., A. Bouhss, D. Mengin-Lecreulx, and D. Blanot.** 2006. The MurE synthetase from *Thermotoga maritima* is endowed with an unusual D-lysine adding activity. J. Biol. Chem. **281:**15680–15686.
5. **Born, T. L., and J. S. Blanchard.** 1999. Structure/function studies on enzymes in the diaminopimelate pathway of bacterial cell wall biosynthesis. Curr. Opin. Chem. Biol. **3:**607–613.
6. **Chaput, C., A. Labigne, and I. G. Boneca.** 2007. Characterization of *Helicobacter pylori* lytic transglycosylases Slt and MltD. J. Bacteriol. **189:**422–429.
7. **Costa, K., G. Bacher, G. Allmaier, M. G. Dominguez-Bello, L. Engstrand, P. Falk, M. A. de Pedro, and F. Garcia-del Portillo.** 1999. The morphological transition of *Helicobacter pylori* cells from spiral to coccoid is preceded by a substantial modification of the cell wall. J. Bacteriol. **181:**3710–3715.
8. **de Pedro, M. A., J. C. Quintela, J.-V. Höltje, and H. Schwarz.** 1997. Murein segregation in *Escherichia coli*. J. Bacteriol. **179:**2823–2834.
9. **de Pedro, M. A., K. D. Young, J.-V. Höltje, and H. Schwarz.** 2003. Branching of *Escherichia coli* cells arises from multiple sites of inert peptidoglycan. J. Bacteriol. **185:**1147–1152.
10. **Dworkin, M., and S. M. Gibson.** 1964. A system for studying microbial morphogenesis: rapid formation of microcysts in *Myxococcus xanthus*. Science **146:**243–244.
11. **Fiegna, F., Y. T. Yu, S. V. Kadam, and G. J. Velicer.** 2006. Evolution of an obligate social cheater to a superior cooperator. Nature **441:**310–314.
12. **Foster, H. A., and J. H. Parish.** 1973. Ribosomes, ribosomal subunits and ribosomal proteins from *Myxococcus xanthus*. J. Gen. Microbiol. **75:**391–400.
13. **Foster, H. A., and J. H. Parish.** 1973. Synthesis of RNA during myxospore induction in *Myxococcus xanthus*. J. Gen. Microbiol. **75:**401–407.
14. **Glauner, B.** 1988. Separation and quantification of muropeptides with high-performance liquid chromatography. Anal. Biochem. **172:**451–464.
15. **Glauner, B., J.-V. Höltje, and U. Schwarz.** 1988. The composition of the murein of *Escherichia coli*. J. Biol. Chem. **263:**10088–10095.
16. **Harcke, E., F. Massow, and H. Kuhlwein.** 1975. On the structure of the peptidoglycan of cell walls from *Myxobacter* AL-1 (*Myxobacterales*). Arch. Microbiol. **103:**251–257.
17. **Harz, H., K. Burgdorf, and J.-V. Höltje.** 1990. Isolation and separation of the glycan strands from murein of *Escherichia coli* by reversed-phase high-performance liquid chromatography. Anal. Biochem. **190:**120–128.
18. **Inouye, M., S. Inouye, and D. R. Zusman.** 1979. Biosynthesis and self-assembly of protein S, a development-specific protein of *Myxococcus xanthus*. Proc. Natl. Acad. Sci. USA **76:**209–213.
19. **Johnson, R. Y., and D. White.** 1972. Myxospore formation in *Myxococcus xanthus*: chemical changes in the cell wall during cellular morphogenesis. J. Bacteriol. **112:**849–855.
20. **Kaiser, D., C. Manoil, and M. Dworkin.** 1979. Myxobacteria: cell interactions, genetics, and development. Annu. Rev. Microbiol. **33:**595–639.
21. **Kottel, R. H., K. Bacon, D. Clutter, and D. White.** 1975. Coats from *Myxococcus xanthus*: characterization and synthesis during myxospore differentiation. J. Bacteriol. **124:**550–557.
22. **Kottel, R. H., M. Orlowski, D. White, and J. Grutsch.** 1974. Presence of amino acid dehydrogenases and transaminases in *Myxococcus xanthus* during vegetative growth and myxospore formation. J. Bacteriol. **119:**650–651.
23. **Kroos, L.** 2007. The bacillus and myxococcus developmental networks and their transcriptional regulators. Annu. Rev. Genet. **41:**13–39.
24. **Labischinski, H., E. W. Goodell, A. Goodell, and M. L. Hochberg.** 1991. Direct proof of a "more-than-single-layered" peptidoglycan architecture of *Escherichia coli* W7: a neutron small-angle scattering study. J. Bacteriol. **173:**751–756.
25. **Leutgeb, W., and U. Schwarz.** 1967. Abbau des Mureins als erster Schritt beim Wachstum des Sacculus. Z. Naturforsch. **22b:**545–549.
26. **Markiewicz, Z., B. Glauner, and U. Schwarz.** 1983. Murein structure and lack of DD- and LD-carboxypeptidase activities in *Caulobacter crescentus*. J. Bacteriol. **156:**649–655.
27. **Nariya, H., and M. Inouye.** 2008. MazF, an mRNA interferase, mediates programmed cell death during multicellular *Myxococcus* development. Cell **132:**55–66.
28. **Nilsen, T., A. S. Ghosh, M. B. Goldberg, and K. D. Young.** 2004. Branching sites and morphological abnormalities behave as ectopic poles in shape-defective *Escherichia coli*. Mol. Microbiol. **52:**1045–1054.
29. **Noens, E. E., V. Mersinias, B. A. Traag, C. P. Smith, H. K. Koerten, and G. P. van Wezel.** 2005. SsgA-like proteins determine the fate of peptidoglycan during sporulation of *Streptomyces coelicolor*. Mol. Microbiol. **58:**929–944.
30. **Okano, P., K. Bacon, and E. Rosenberg.** 1970. Ribonucleic acid synthesis during microcyst formation in *Myxococcus xanthus*: characterization by deoxyribonucleic acid-ribonucleic acid hybridization. J. Bacteriol. **104:**275–282.
31. **Orlowski, M., P. Martin, D. White, and M. C. Wong.** 1972. Changes in activity of glyoxylate cycle enzymes during myxospore development in *Myxococcus xanthus*. J. Bacteriol. **111:**784–790.
32. **Orlowski, M., and D. White.** 1974. Inactivation of isocitrate lyase during myxospore development in *Myxococcus xanthus*. J. Bacteriol. **118:**96–102.
33. **Popham, D. L.** 2002. Specialized peptidoglycan of the bacterial endospore: the inner wall of the lockbox. Cell. Mol. Life Sci. **59:**426–433.
34. **Popham, D. L., J. Helin, C. E. Costello, and P. Setlow.** 1996. Muramic lactam in peptidoglycan of *Bacillus subtilis* spores is required for spore outgrowth but not for spore dehydration or heat resistance. Proc. Natl. Acad. Sci. USA **93:**15405–15410.
35. **Prats, R., and M. A. de Pedro.** 1989. Normal growth and division of *Escherichia coli* with a reduced amount of murein. J. Bacteriol. **171:**3740–3745.
36. **Quintela, J. C., M. Caparros, and M. A. de Pedro.** 1995. Variability of

peptidoglycan structural parameters in gram-negative bacteria. FEMS Microbiol. Lett. **125:**95–100.
37. **Reichenbach, H.** 1999. The ecology of the myxobacteria. Environ. Microbiol. **1:**15–21.
38. **Rhuland, L. E., E. Work, R. F. Denman, and D. S. Hoare.** 1955. The behaviour of the isomers of α,ε-diaminopimelic acid on paper chromatograms. J. Am. Chem. Soc. **77:**4844–4846.
39. **Rosenberg, E., M. Katarski, and P. Gottlieb.** 1967. Deoxyribonucleic acid synthesis during exponential growth and microcyst formation in *Myxococcus xanthus*. J. Bacteriol. **93:**1402–1408.
40. **Schleifer, K. H., and O. Kandler.** 1972. Peptidoglycan types of bacterial cell walls and their taxonomic implications. Bacteriol. Rev. **36:**407–477.
41. **Sudo, S., and M. Dworkin.** 1972. Bacteriolytic enzymes produced by *Myxococcus xanthus*. J. Bacteriol. **110:**236–245.
42. **Sudo, S. Z., and M. Dworkin.** 1969. Resistance of vegetative cells and microcysts of *Myxococcus xanthus*. J. Bacteriol. **98:**883–887.
43. **Takahashi, Y., Y. Iwai, and S. Omura.** 1984. Two new species of the genus *Kitasatosporia*, *Kitasatosporia phosalacinea* sp. nov and *Kitasatosporia griseola* sp. nov. J. Gen. Appl. Microbiol. **30:**377–387.
44. **Varma, A., and K. D. Young.** 2004. FtsZ collaborates with penicillin binding proteins to generate bacterial cell shape in *Escherichia coli*. J. Bacteriol. **186:**6768–6774.
45. **Vollmer, W.** 2008. Structural variation in the glycan strands of bacterial peptidoglycan. FEMS Microbiol. Rev. **32:**287–306.
46. **Vollmer, W., D. Blanot, and M. A. de Pedro.** 2008. Peptidoglycan structure and architecture. FEMS Microbiol. Rev. **32:**149–167.
47. **Vollmer, W., and J.-V. Höltje.** 2004. The architecture of the murein (peptidoglycan) in Gram-negative bacteria: vertical scaffold or horizontal layer(s)? J. Bacteriol. **186:**5978–5987.
48. **Vollmer, W., B. Joris, P. Charlier, and S. Foster.** 2008. Bacterial peptidoglycan (murein) hydrolases. FEMS Microbiol. Rev. **32:**259–286.
49. **Watson, B. F., and M. Dworkin.** 1968. Comparative intermediary metabolism of vegetative cells and microcysts of *Myxococcus xanthus*. J. Bacteriol. **96:**1465–1473.
50. **Wehrmann, A., B. Phillipp, H. Sahm, and L. Eggeling.** 1998. Different modes of diaminopimelate synthesis and their role in cell wall integrity: a study with *Corynebacterium glutamicum*. J. Bacteriol. **180:**3159–3165.
51. **Weidel, W., and H. Pelzer.** 1964. Bag shaped macromolecules—a new outlook on bacterial cell walls. Adv. Enzymol. **26:**193–232.
52. **White, D., M. Dworkin, and D. J. Tipper.** 1968. Peptidoglycan of *Myxococcus xanthus*: structure and relation to morphogenesis. J. Bacteriol. **95:**2186–2197.
53. **Wientjes, F. B., C. L. Woldringh, and N. Nanninga.** 1991. Amount of peptidoglycan in cell walls of gram-negative bacteria. J. Bacteriol. **173:**7684–7691.
54. **Wireman, J. W., and M. Dworkin.** 1975. Morphogenesis and developmental interactions in myxobacteria. Science **189:**516–523.
55. **Zusman, D., and E. Rosenberg.** 1968. Deoxyribonucleic acid synthesis during microcyst germination in *Myxococcus xanthus*. J. Bacteriol. **96:**981–986.